Effect of plasmonic Au nanoparticles on red $^5D_0 \rightarrow {}^7F_2$ electric dipole emission transition of Eu^{3+} ions in low phonon antimony based dichroic metallo-dielectric nanocomposites

Tirtha Som, Basudeb Karmakar*

Glass Science & Technology Section, Glass Division,
Central Glass and Ceramic Research Institute
(Council of Scientific and Industrial Research (CSIR), India)
196 Raja S. C. Mullick Road, Kolkata 700 032, India

Abstract

Eu^{3+} ions and elliptical Au nanoparticles incorporated new antimony based reducing dielectric (here glass) matrix, K_2O-B_2O_3-Sb_2O_3 (KBS), has been prepared by a new single-step methodology involving selective thermochemical reduction without employing any external reducing agent. X-ray diffraction (XRD) and selected area electron diffraction (SAED) results of these hybrid nanocomposites indicate that Au^0 nanoparticles are grown along the (111) and (200) plane direction. The transmission electron microscopic (TEM) image reveals formation of elliptical Au^0 nanoparticles of major axis (diagonal) 5 to 12 nm range. Dichroic behavior is due to elliptical shape of Au^0 nanoparticles having aspect ratio of about 1.2. Presence of Au nanoparticles introduces a local crystalline environment and perturbs the local site symmetry around the Eu^{3+} ions resulting in well-resolved stark splitting of the electric dipole $^5D_0$–$^7F_2$ emission transition into two components (617 and 640 nm). The photoluminescence intensity of the 640 nm red emission of Eu^{3+} drastically enhances by ~ 8 folds in presence of Au^0 nanoparticles and then attenuates with further increase in Au^0 concentration. This advocates two types of nano Au^0 distribution, clustered and dispersed sites, around the Eu^{3+} ions. On the contrary, the magnetic dipole $^5D_0$–$^7F_1$ orange (596 nm) transition remain almost unaffected by the presence of nano Au^0. Local field enhancement induced by plasmonic Au^0 is found to be

responsible for the enhancement while reverse energy transfer from $Eu^{3+} \rightarrow Au^0$ and optical re-absorption due to Au^0 surface plasmon resonance for attenuation.

PACS number(s): 42.70.Ce, 78.55.-m, 42.70.Hj, 42.79.-Nv, 78.20.-e.

Keywords: Nano gold; Europium (III); Nanocomposite; Enhanced photoluminescence; Dichroic; Antimony oxide glass

---

*Corresponding author. Tel: +91-33 2473 3469; fax: +91-33 2473 0957

E-mail address: basudebk@cgcri.res.in (B. Karmakar)

1. Introduction

Luminescence study from rare-earth (RE) ions or lanthanides has received startling interest because of their continuously expanding applications in environment friendly solid state lighting, electroluminescent devices, luminescent sensors, optical information storage, solar cells, etc [1,2]. Among the REs, the europium (Eu^{3+}) ion is actively used as an efficient down-converting red-light emitting center for display devices [3]. For solar cell applications also, a down-converting layer placed in front of a silicon solar cell has the potential to generate more than one low-energy (visible) photon for every incident high-energy (UV) photon, thereby modifying the incoming spectrum, but many challenges remain. Very recently, the urges to develop advanced displays, LEDs and solar cells have provoked the synthesis of new highly luminescent hybrid materials co-embedding RE^{3+} ions and metal nanoparticles (NPs) [4-7].

Coinage metal NPs (like Au and Ag) embedded in dielectrics (here glass) exhibit the remarkable opto-electronic phenomenon of "surface plasmon resonance" (SPR) in the visible region. SPR is the collective oscillation of metal valence electrons or plasmas with respect to the ionic core of the nanoparticle resonantly excited by electromagnetic radiation due to electronic confinement effects [4]. The results associated with SPR are strong absorption bands, intense light scattering and tremendous enhancement of the local electromagnetic field [4]. The local field enhancement may be so strong that luminescent species in the vicinity of the plasmonic nanoparticle may experience 100 times more intense field compared to direct excitation in a plasmon-free environment [5]. This enhanced near-fields around metallic nanostructures have facilitated a variety of intriguing applications such as non-linear optics, surface-enhanced Raman scattering (SERS), single-molecule detection (spectroscopy), nano-metal enhanced luminescence (NMEL) (fluorescence as well as phosphorescence), etc [8].

Much inspired by the discovery of SERS in 1974, Malta et al. [9] first studied luminescence of the Eu^{3+} ions in presence of silver NPs in fluoro-borate glasses prepared by conventional glass-melting technique but incorporating a small quantity of Sb_2O_3 (1.5 and 3 %) to assists in the reduction of Ag^+ ions to Ag NPs. They deduced the phenomenon as silver plasmonic enhancement effect and long range electromagnetic interactions associated with SPR excitation. Their results were supported by Hayakawa et al [10]. They investigated luminescence enhancement of Ag NPs–Eu^{3+} ions co-doped sol-gel derived silica glasses (prepared by using partially hydrolyzed tetrakis(hydroxymethyl) phosphonium chloride as the reducing agent and annealing in hydrogen atmosphere) and found that irrespective of Ag concentration, the decay from the $^5D_0$ level of Eu^{3+} almost have the same life-time. The lifetime of plasma oscillation of Ag NPs (10^{-4}s) is much smaller than that of Eu^{3+} ions (10^{-3}s). Consequently, Hayakawa et al. [10] also overruled the possibility of energy transfer from Ag NPs to Eu^{3+} ions. Thereafter, several researchers worldwide took up NMEL studies of Er^{3+}, Sm^{3+}, Tb^{3+}, Eu^{3+}, Dy^{3+}, etc ions by monometallic Au or Ag NPs in glasses and other dielectric offering the possibilities of plamon induced nanphotonics engineering [5,7,11-16]. However, the simultaneous studies also led to several controversies related to metal–RE interactions in a dielectric host and the mechanism of photoluminescence enhancement.

Here it must be emphasized that the conventional methodologies of fabrication of metal-glass nanocomposites are multi-step. They involve sol-gel, ion-exchange, ion-implantation, sputtering deposition in the first step to incorporate the metal ions in the dielectrics followed by long time heat treatments in reducing atmosphere, laser irradiation, etc to reduce them [7,10,11,17]. Strohhöfer and Polman [11] reported the photoluminescence enhancement of Er^{3+} ions implanted in boro-silicate glasses that had been subjected to $Na^+ \leftrightarrow Ag^+$ ion exchange via

absorption at a defect centre related to silver ions/atoms and energy transfer towards Er^{3+}. Matarelli et al. [7] described electric-dipole induced energy transfer process from ionic silver aggregates, particularly dimmers, accounting the enhancement of 1.52 μm emission of Er^{3+} in silver-doped silicate glasses fabricated by ion-exchange technique. These contrasting conclusions are probably induced by the fact that silver ions introduced in glasses by conventional ion-exchange or ion-implantation are very mobile and with heat treatment have a strong tendency to aggregate not only resulting in NPs, but single ions, cluster of few atoms (dimers, trimers, etc.), and other luminescent centers like (Ag^+, $(Ag_2)^+$, $(Ag^+)_2$, $(Ag_3)^{2+}$) [16]. Matarelli et al. [7] have revealed that the distribution of different active species related to the incorporated silver, observed from their photoluminescence spectral signatures, depends on heat treatment schedule and silver concentration. The SPR band at 420 nm, typical of the spheroidal silver NPs in silicate glasses, is observable only after heating at 600 °C in air for long duration.

Metal NPs may enhance the RE-luminescence by local field enhancement when the pumping excitation or emission is resonant or lies near the SPR wavelength [12]. Fukushima et al [13] have observed dramatic enhancement of 1.53-μm emission from Er-doped sol-gel SiO_2 films by Au nanoparticles doping upon 520 nm resonant Er^{3+}-excitation. The wavelength of 520 nm corresponds to $^4I_{15/2} \rightarrow {}^2H_{11/2}$ excitation of Er^{3+} and also resonant with SPR maxima of Au in SiO_2 matrix. They have attributed not only to local field enhancement but also to enhancement of absorption cross-section of Er^{3+} due to localized SPR of Au NPs. Kassab et al [14,15] recognized both local field enhancement and energy transfer from Au NPs as contributing factors to photoluminescence intensification of Eu^{3+} ions under 405 nm excitation as this wavelength is not only resonant with the $^7F_0 \rightarrow {}^5D_3$ Eu^{3+} transition but also overlap with Au SPR band in GeO_2–Bi_2O_3 glass. Therefore, although the differentiation between the different luminescence

enhancement mechanisms has remained disputed, now it is evident that it is the technique which is employed to generate the NPs in glasses plays a vital role.

Studies on the influence of metal NPs on Eu(III)-complex in solution have revealed quenching at higher concentration of metal [18,19]. Thus, plasmon enhanced fluorescence results from two competing processes, increased excitation rate of the RE^{3+} ions due to local field enhancement and quenching due to energy transfer by the excited RE^{3+} ions to the metal surface. Hence, there must exist a critical distance from the metal surface where the fluorescence enhancement is largest. The photoluminescence enhancement is also governed by nanoparticles' morphology, dimension and number density, inter-particle distance and other environmental parameters [4,8,18,19]. The field enhancement for a non-spherical (anisotropic) nanoparticle is considerably greater than that of a spherical particle of comparable size [4,20]. The local surface charge densities are drastically increased and confined near the sharp edges of anisotropic nanostructures (ellipsoids, hexagons, nanorods, triangles, etc.) leading to crowding of electric fields. This phenomenon, termed as "lightning-rod effect", enables the sharp edges to act as light-harvesting nano optical antennas converting visible light into large localized electric field. [4,20]. However, the fabrication of glasses containing plasmonic monodisperse NPs, particularly the anisotropic ones is not straightforward. The conventional methodologies of metal-glass nanocomposite fabrication yield mainly spherical NPs.

But to the best of our knowledge, there is no report of NMEL of Eu^{3+} ions in antimony oxide (Sb_2O_3) glass matrix This is primarily due to the difficulties preparation of Sb_2O_3 glasses in the bulk monolithic form owing to the high volatility of the melts, intense crystallization during cooling, and inefficiency of Sb_2O_3 to form glass network due to low field strength of Sb^{3+} (0.73). Application of forced cooling or quenching techniques do yield high antimony containing

glasses but usually as tiny pieces incompatible for real photonic applications [21]. These have drastically hindered the exploitation of Sb_2O_3-based glasses for photonic studies. In fact Sb_2O_3-based glasses have been rarely studied. It is only in recent times we first developed monolithic antimony glasses in the system K_2O-B_2O_3-Sb_2O_3 [21] and exploited the photoluminescence properties of Eu^{3+} ions in these glasses which remarkably showed unusual features [22]. Like other heavy metal oxide glasses, Sb_2O_3 glasses also possess inherent advantages like high refractive index, low phonon energy (602 cm^{-1}), large transmission windows (about 0.35-6.5 μm) and large non-linear optical properties [21,22]. But the most significant aspect of Sb_2O_3 based glasses over others is that Sb_2O_3 is a mild reducing agent [23] and it enables selective reduction of Au^{3+} ($HAuCl_4.xH_2O$) to Au^0 than RE (Eu^{3+}) ions (Eu_2O_3) in a single-step during the melting process thereby providing for a straightforward, low-cost strategy for the fabrication of bulk nano metal: RE^{3+} hybrid nanocomposites for application in nanophotonic technologies.

Pondering on the above issues, we demonstrate in this paper the single-step melt-quench route for fabrication of a new RE (Eu^{3+})-metallo-dielectric hybrid nanocomposite, that is, bulk potassium boron antimony oxide glass (mol %) $15K_2O$-$15B_2O_3$-$70Sb_2O_3$ (KBS) co-doped with elliptical gold (Au^0) NPs and Eu^{3+} ions, involving thermochemical reduction by employing the reducing property of Sb_2O_3 and metal cluster chemistry simultaneously. We also attempt to realize the effect of Au^0 NPs on the fluorescence emissions (visible) of Eu^{3+} ions under photoexcitation of UV (violet) light, thus study plasmonic controlled nanophotonics in these nanocomposites and explain them with the existing fundamental (electrodynamics) theories. The resultant hybrid nanocomposites were also characterized by X-ray diffraction (XRD) analysis and transmission electron microscopy (TEM) as well.

2. Experimental Details

We used potassium metaborate, $KBO_2.xH_2O$ (15.7% H_2O, Johnson Matthey), antimony(III) oxide, Sb_2O_3 (GR, 99 %, Loba Chemie), chloroauric acid, $HAuCl_4.xH_2O$ (49 % Au, Loba Chemie), and europium(III) oxide, Eu_2O_3 (99.99 %, Alfa Aesar) as raw materials. 20 g base glass of composition (mol %) $15K_2O$-$15B_2O_3$-$70Sb_2O_3$ (KBS) was melted using these raw materials in a high purity silica crucible at 900ºC in air. The molten glass was cast onto a carbon plate and properly annealed. The nanocomposites were prepared in a similar technique using respective dopants (in excess) as shown in Table 1. Samples of about 2.0 ± 0.05 mm thickness were polished for optical measurements.

The density of the glasses was measured by Archimedes method using toluene with an error of ± 0.7 %. X'pert Pro MPD diffractometer operating at 40 kV and 30 mA employing Ni-filtered Cukα radiation was used to record the X-ray diffraction patterns of the bulk samples with step size 0.05º (2θ) step time 0.5 sec, from 10 to 80º. TEM was done using a Jeol JEM 2010 operating at 200 kV. Lambda 20 double-beam spectrophotometer was used to trace the UV-Vis-NIR absorption spectra at normal incidence with unpolarized light at a band position error of ± 0.1 nm. Fluorescence spectra were measured, at ± 0.2 nm error, with a Spex Fluorolog 2 spectrophotometer with a Xenon lamp as excitation source and a photomultiplier tube as detector. The excitation slit (1.25 mm) and emission slit (0.5 mm) were kept same for all samples. All measurements were carried out at room temperature. The enhancement of luminescence was found to be reproducible for all samples.

3. Results and discussion

3.1 Mechanism of thermochemical reduction

For simple systems, at room temperature, the standard reduction potentials (E°) of the redox systems are Sb^{5+}/Sb^{3+} (E° = 0.649 V), Au^{3+}/Au^{0} (E° = 1.498V), Eu^{3+}/Eu^{0} (E° = -1.991 V), Eu^{3+}/Eu^{2+} (E° = -0.36 V) and Eu^{2+}/Eu^{0} (E° = -2.812 V) [23]. A probable mechanism of selective thermo-chemical reduction of Au^{3+} to Au^{0} by Sb^{3+} and not reduction of Eu^{3+} by Sb^{3+} can be explained by considering these E° values. Here the only feasible spontaneous reduction reaction is $3Sb^{3+} + 2Au^{3+} \rightarrow 3Sb^{5+} + 2Au^{0}$ (E° = 1.05 V, $\Delta G = -nE°F$, and hence, calculated free energy (ΔG) is around -608 kJ). Thus, Sb^{3+} reduce Au^{3+} to Au^{0}, while it itself is oxidized to Sb^{5+}. Other reactions like $3Sb^{3+} + 2Eu^{3+} \rightarrow 3Sb^{5+} + 2Eu^{0}$ and $Sb^{3+} + 2Eu^{3+} \rightarrow Sb^{5+} + 2Eu^{2+}$ would have an E° values -5.93 and -1.37 V respectively (ΔG is positive) manifesting that these reactions are non-spontaneous and thermodynamically not feasible. Thus Eu^{3+} is not reduced. The E° of polyvalent elements in glass melts may be different from those in aqueous solutions and dependent on temperature. The E° values for antimony glasses at high temperature are unavailable in literature, so the room temperature E° for simple systems at equilibrium with air is considered here.

3.2 Physical properties

The composition and some properties of monolithic nanocomposites are listed in Table 1. The yellow color of the Eu^{3+} doped glass is due to the combined effects of host absorption due to transition between HOMO (Sb 5s + O 2pπ) and LUMO (Sb 5p) and the extended tails of charge transfer band of Eu-O around 240 nm [21,22]. Interestingly, all Au-doped nanocomposites were dichroic, i.e., they transmitted the green to blue (Fig. 1a) color and reflected the brown light (Fig. 1b). The intensity of the reflected brown color increases with increase in Au^{0} concentration.

3.3 X-ray diffraction analysis

The XRD patterns of the Eu^{3+} doped glass, E (Fig. 2, curve a) shows absence of sharp peaks emphasizing its amorphicity. The Eu^{3+}:Au hybrid nanocomposites EG1, EG2 and EG3 (curves b, c and d respectively) show prominent diffraction peaks of Au at 2θ = 38.4021° (d = 2.34216 Å) and 44.1634° (d = 2.04906 Å) can be indexed as the diffractions from (111) and (200) plane of Au crystals (JCPDS Card File No. 4-0784) embedded in KBS antimony glass matrix. The Scherrer's formula was used to calculate average diameter (D) Au^0 nanocrystallites [24]:

$$D = 0.9\lambda/\text{FWHM} \cos 2\theta \text{ (peak)} \quad (1)$$

where λ is the wavelength of X-ray radiation (CuKα = 1.5406Å), FWHM is the full width at half maximum at 2θ. They are listed in Table 1 and are found to be varied in the range 10-26 (± 1) nm. The XRD patterns also indicate the complete reduction of Au^{3+} to Au^0 by Sb_2O_3 since there is no other Au-containing species.

3.4 TEM and SAED analyses

The TEM photograph (Fig. 3a) of nanocomposite EG1 shows closely dispersed Au^0 NPs, majority of which have elliptical morphology. Besides there are two types of Au NPs sites—clustered and dispersed. These elliptical NPs have maximum length (major axis) ranging from 5 to 12 nm (± 3 %) and aspect ratio of about 1.2. It is probably the influence of the high viscosity of the molten Sb_2O_3 based matrix on the Au^0 colloids which results in the formation of elliptical nanoparticles.

For sample EG1, the slight discrepancy between the TEM image and that calculated from Scherrer formula (Table 1) is due to the fact that the TEM image represents a particular section

where as the average diameter of the Au nanocrystllites is evaluated using the Scherrer equation (XRD patterns).

The SAED image (Fig. 3b) shows the presence of (111) and (200) crystallographic planes of Au^0 NPs and agrees well with the XRD patterns (Fig. 2).

3.5 UV-Vis-NIR absorption spectra

The absorption peaks of Eu^{3+} are not easily discernible in the absorption spectra. The inset of Fig. 4 can help in the detection of the absorption peaks. The absorption spectrum of Eu^{3+} ions in KBS antimony glass (Fig. 4 curve-a and inset) shows six apparently resolved absorption bands at 393, 463, 526, 533, 578 and 586 nm due to $^7F_0 \rightarrow {}^5L_6$, $^7F_0 \rightarrow {}^5D_2$, $^7F_0 \rightarrow {}^5D_1$, $^7F_1 \rightarrow {}^5D_1$, $^7F_0 \rightarrow {}^5D_0$ and $^7F_1 \rightarrow {}^5D_0$ transitions respectively. The assignment of these transitions has been done on the basis of the energy level positions of Eu^{3+} ions in aqueous solution [25]. At low temperature, the absorption spectrum in the UV-Vis region usually arises due to transitions from the $^7F_0$ ground state to the ^5D_J (J = 0, 1, 2 and 3) multiplets. Since $^4F_1$ level, multiplet of the ground $^7F_0$ level, is only about 243 cm^{-1} above the $^7F_0$ level, so at room temperature transitions from the $^4F_1$ level is also observed due to thermal population. The absorption bands below 360 nm are cut off by the absorption of the base KBS antimony glass. The intensity of the $^7F_0 \rightarrow {}^5D_1$ (526 nm) absorption band is very weak because it is magnetic dipole (MD) allowed transition while the intensity of the hypersensitive $^7F_0 \rightarrow {}^5D_2$ (463 nm) electric dipole (ED) induced transition is relatively very strong. The electric dipole $^7F_0 \rightarrow {}^5L_6$ transition (393 nm) is also weak because it is forbidden by the ΔS and ΔL selection rules but allowed by the ΔJ selection rule. An induced electric dipole transition from a level having $J = 0$ to $J' = 0$ is forbidden but crystal field splitting in the host consequences in J-mixing and makes the $^7F_0 \rightarrow {}^5D_0$ transition partially

feasible. Consequently in our KBS antimony glass host, the $^7F_0 \rightarrow {}^5D_0$ (533 nm) transition has a very low intensity.

The Au^0 and Eu^{3+} co-doped nanocomposites (Fig. 4, curves b, c and d) displays broad plasmon (SPR) absorption bands distinctive of nano sized Au^0 in addition to the inherent absorption peaks of Eu^{3+}. The Au SPR band in our KBS antimony glass appears at 609 nm (sample EG1, curve b), which is a drastic red-shift by 89 nm as compared to the usual 520 nm SPR position in sodalime silicate glasses. As a result they overlap with orange and red emissions of Eu^{3+} ions. It is known that SPR is critically dependent on the nanoparticle size, shape, refractive index of the dielectric environment and other proximal NPs [26]. The SPR peaks generally experience a red-shift as the refractive index of the surrounding environment is increased [26]. This is because with increasing dielectric constant of the surrounding host due to the increase of polarization charges on the dielectric side of the interface, the overall restoring force goes on deteriorating. The refractive index (n) of sodalime silicate glasses is about 1.5 while that of KBS glass it is 1.9477. Moreover non-spherical metal NPs also red-shifted compared to spherical ones [4]. So, the dramatic red-shift is primarily due to the change in refractive index of the host glass and deviation of particle shape from spherical ones [4,8,26].

The absorption is higher as the Au concentration increases. This is because the increase of metallic gold within the glasses greatly reduces the transmission in the visible range. The maxima of the plasmon bands (λ_{max}), as listed in Table 1, have experience a distinctive red-shift towards higher wavelength (from 609 nm to 679 nm) with increase in Au concentration (from 0.003 to 0.3 wt %). In addition the SPR bands have gradually broadened and have become asymmetric with their tails extending up to 1100 nm. The SPR band broadening probably arises from a distribution of elongated particles with different long axis [4].

3.6 Dichroic behavior

The origin of dichroism in nano-structuted materials is a controversial topic yet to be clarified. Earlier researchers had observed dichroism in Saphirin glass (silicate and borosilicate base glasses containing both small 5-60 nm and large 200-500 nm size Au nanoparticles) [27], that gave blue color in the transmitted and brown color in the reflected light and absorption wavelength shifts from 530 to 570 nm with successive crystal growth. It was believed that dichroism originated from scattering and reflection of light by the large size Au NPs. Later on, the advent of commercial TEM made possible the determination of actual shapes of gold particles. Particles which are sufficiently large and which deviate in shape from sphere orient themselves parallel and produce birefringence.

Production of dichroic glasses currently involves deformation (stretching) of embedded spherical nanoparticles into oblong or ellipsoidal NPs by intense irradiation with ultrashort laser pulses [28] or high intensity ion/ electron bean irradiation [29] or stretching metal-doped glasses in their softening range [30]. Hofmeister and his coworkers [31] have produced silicate based dichroic glasses by deformation of embedded spherical nanoparticles into aligned ellipsoidal nanoparticles by these techniques and prolate ellipsoid metal NPs having an aspect ratio around 1.2 exhibits the phenomenon of dichroism..

The high viscosity of the Sb_2O_3 glass melt probably assists in deformation of spherical NPs formed and since this is an in-situ reduction involving single-step melting, so some random orientations of the elliptical particles are also observed. We believe that the dichroism exhibited by the Au-doped antimony glass nanocomposites may be due to the elliptical shape of the Au^0 NPs and arises due to the difference in polarizations, that is, electron polarizations (oscillations) along the major (longitudinal) and minor (transverse) axes of polarizable ellipsoidal NPs during

interaction with incident light wave. [4,31-33]. This can be explained with electrodynamics theory.

For ellipsoidal particles, the extinction cross-section, C_{ext}, of is directly proportional to their imaginary part of polarizability, $\alpha_{x,y,z}$ as [4,31-33]:

$$C_{ext} = 2\pi n_h \, I(\alpha_{x,y,z})/ \lambda \qquad (2)$$

where

$$\alpha_{x,y,z} = \frac{4\pi abc}{3} \frac{\varepsilon_{Au} - \varepsilon_m}{\varepsilon_m + L_{x,y,z}(\varepsilon_{Au} - \varepsilon_m)} \qquad (3)$$

where ε_{Au} and ε_m are the effective dielectric constant of the metal and surrounding matrix respectively. Here, a, b and c denote the length of the ellipsoid along the x, y and z axes (a > b = c) and $L_{x,y,z}$ are the depolarization factors for the respective axis.

Again, $L_x = [(1-e^2) / e^2] [-1 + (1/2e)\ln (1+e)/(1-e)]$ (4)

and $L_{y,z} = (1-L_x)/2$ (5)

where $e = [1- (b/a)^2]^{1/2}$ is the eccentricity of the ellipsoid. For the degenerate case of a sphere e = 0, or $L_{x,y,z} = 1/3$. Under these conditions the birefringence disappears. The implied meaning of is very clear. Oriented ellipsoids exhibit strong polarization-dependent optical spectra. Simply, nanocomposites exhibits dichroic behavior, that is, one color in the transmitted light and a different color in the reflected light.

Moreover, the denominator of Eq. 3 is resonant at the SPR. Consequently, the new SPR position is [4,33]:

$$\varepsilon_{Au} = (-1/Lj + 1) \, \varepsilon_m, \qquad (6)$$

Hence by changing the shape and refractive index of the medium, the SPR can be tuned across a wide spectroscopic region.

3.7 Excitation spectra

The excitation spectrum with emission at 617 nm is presented in Fig. 5. The excitation spectra clearly reflect the band structure of the Eu^{3+} ion between 340 to 570 nm. Among them the intensities of the 393, 463 and 532 nm excitation peaks are reasonably high suggesting the violet, blue and green lasers are promising excitation sources for obtaining utmost fluorescence intensity in spectral conversion process. The assignment of the locations of energy bands has been made with the help of Carnall's convention of Eu^{3+} ion in aqueous solution [25] and earlier studies of Eu^{3+}-doped glasses [1,3,22].

3.8 Photoluminescence spectral conversion

Emission spectrum of 0.3 wt% Eu_2O_3 doped KBS glass, under 393 nm excitation, is shown in Fig. 6 (curve-a). The emission bands at 583 nm (yellow, $^5D_0 \rightarrow {}^7F_0$: zero-zero band), 596 nm (orange, $^5D_0 \rightarrow {}^7F_1$, magnetic dipole transition), 617 nm (red, $^5D_0 \rightarrow {}^7F_2$, electric dipole transition), 654 nm (deep-red, $^5D_0 \rightarrow {}^7F_3$, forbidden), and 704 nm (deep-red, $^5D_0 \rightarrow {}^7F_4$, forbidden). The $^5D_0 \rightarrow {}^7F_1$ (596 and 600 nm) and $^5D_0 \rightarrow {}^7F_2$ (617 and 640 nm) transitions shows two distinctive stark splitting each implicating that the Eu^{3+} ions in the host base glass lie at acentric sites. It is interesting to note that the green emission observed at 536 nm due to $^5D_1 \rightarrow {}^7F_1$ transition, is seldom seen in glass hosts having high phonon energy [1]. This emphasizes that antimony glasses are definitely low phonon ones. Som and Karmakar [21,22] have demonstrated that the phonon energy of KBS antimony glasses is about 602 cm^{-1}, which is very close to that of fluoride glasses.

The energy level diagram of Eu^{3+} ion in KBS glass is given in Fig. 7. When Eu^{3+}-doped KBS antimony glass is excited by 393 nm violet light, the Eu^{3+} ions are first excited to $^5L_6$ level

by ground state absorption. This is followed by rapid multiphonon relaxation from $^5L_6$ to $^5D_0$ level and probably also the $^5D_1$ level to some extent due to the low phonon energy of the glass. The multiphonon relaxation processes from $^5D_1$ to $^5D_0$ levels and from $^5D_0$ to the next lower $^7F_6$ level are accomplished by 3 and 21 bridging phonons respectively. This is according to the relation of the minimum number (p) of maximum energy photons ($\hbar\nu_{max}$) required for a transition between two states separated by an energy gap (ΔE) as given by [1]:

$$p = \Delta E/\hbar\nu_{max} \quad (7)$$

Therefore, both of them ($^5D_1$ and $^5D_0$) require high order of phonons (≥ 3), so effective green and red emissions of Eu^{3+}-doped KBS glass is highly favored. Thus, it can be also argued that multichannel visible emissions of Eu^{3+} in KBS glass due to its low phonon energy and low site symmetry.

The $^5D_0 \rightarrow {}^7F_{1,3}$ transitions are magnetic-dipole (MD) allowed and are not much sensitive to changes in the crystal field environment of the host matrix and are also forbidden under selection rules [3,22,34]. Conversely, $^5D_0 \rightarrow {}^7F_{2,4}$ emission transitions are allowed by electric-dipole (ED) and are enforced by the crystal field environment in the vicinity of the Eu^{3+} ions 3,22,34]. Consequently, their amplitudes are susceptible to changes in the polarizability of the ligand and reduction of the local symmetry around the Eu^{3+} ions. The emission spectra are indicative of the rare-earth sites. Kassab et al [14,15] have showed that the dominant hypersensitive $^5D_0 \rightarrow {}^7F_2$ electric dipole (red) transition is increased by 10 fold by Au NPs while the less sensitive $^5D_0 \rightarrow {}^7F_1$ magnetic dipole (orange) transition is enhanced only by 5 folds.

We observe a change of the emission profile with the introduction of Au and change in its concentration (Fig. 6, curves b-d). The formation of Au nanocrystallites introduces local crystalline environment and perturbs the local site symmetry resulting in well resolved Stark's

splitting of the hypersensitive ($\Delta J=2$) $^5D_0 \rightarrow {}^7F_2$ red emission transition (617 and 640 nm) due to crystal field effect, as observed in the emission transitions of Eu^{3+} ions. The crystal field from the host influences the transitions probabilities between the rare earth levels in a way dependent of the microscopic details of the quantum charge distributions. The principal result of the current study is that the 640 nm (deep-red) fluorescence of Eu^{3+} initially drastically enhances in presence of Au^0 NPs and then diminishes at very high Au concentration. This behavior is illustrated in Figs. 6 and 8, and Table 2. This implicate that trivalent Eu^{3+} ions are located at least into two different crystalline environments, namely, a clustered crystalline environment and dispersed one as indicated in Fig. 3 (TEM image) [34,35].

We believe that the enhanced luminescence is primarily due to local field enhancement (LFE) around the Eu^{3+} ions induced by SPR of Au NPs [4-6,9,10,12-15]. We may exclude energy transfer from Au NPs to Eu^{3+} ions as the excitation wavelength does not overlay the SPR absporption, which therefore cannot be the initial step in the excitation of Eu^{3+}. Glasses incorporating silver or gold by conventional techniques (ion-implantation, ion-exchange or sol-gel and subsequent heat-treatment) also embed isolated ions, ionic clusters or metal oxides in addition to very small quantity of NPs. TEM and XRD detect only formed particles, whereas only ions or small clusters are detected by luminescence study. Absorption bands of Au^+ and Ag^+ ions in glasses are centered at about 325 and 250 nm respectively in the UV region and they can be identified by their characteristic photoluminescence. Shin et al. have observed a fluorescence band at 430 nm in Au-doped borate glasses and have attributed it to Au^+ ions in the partially reduced nanoclusters [36]. Wilcoxon et al. [37] had reported that luminescent gold clusters had no SPR absorption, but in case of fully reduced Au NPs in solution, when a broad and strong SPR absorption band existed in the UV-vis region, no emission was observed. Similarly, for

silver, broad emission bands at around 380 and 600 nm are generally attributed isolated Ag^+ ions and Ag^+-Ag^+ pairs emissions respectively whereas emission centered around 445 nm under ~275 and ~375 nm excitation originates due to $4d^{10}5s^1 \leftrightarrow 4d^{10}5p^1$ transitions of $(Ag_2)^+$ pairs which are the nucleation centers in the precipitation of silver nanoclusters [38]. On the contrary, Ag NPs does not exhibit luminescence in the visible region. Our luminescence experiments indicated the absence of any other optical centers. Apart from the Eu^{3+} emission bands, we did not obtain any other emission band under excitation at various wavelengths which could be ascribed to any Au ionic species [39]. Moreover, the excitation spectrum obtained at 640 nm excitation yielded only the excitation bands of Eu^{3+} ions. This is because we used exceedingly large quantity of reducing agent (89.25 wt% Sb_2O_3) compared to $HAuCl_4.H_2O$ (0.003-0.3 wt% Au). Therefore, we can exclude the co-existence of various ionic species which as serve as optical centers. Based on this argument we may also eliminate the energy transfer to Eu^{3+} ions from ionic Au.

With regard to the origin of the spatially localized enhanced electric field around the metallic nanostructures, the difference between the dielectric constants of the metallic NPs and the host glass is regarded as the probable cause [4,20]. SPR generates electromagnetic waves that propagate only along the surface of the metal, i.e. metal-dielectric interface. They are trapped on the surface because of the interaction with the free electrons of the conductor (metal) [20]. Thus surface plasmons help to concentrate as well as channel light in sub-wavelength structures. Concentration of light results in electric field enhancement in the vicinity of metal nanostructures that can be used to manipulate and boost several phenomenons (e.g. NMEL). The SPR allows electromagnetic energy to be concentrated at inter-particle junctions. These inter-particle junction regions, termed as “hot spots”, exhibits highly confined giant local fields [4,8,20]. RE^{3+} ions or luminescent molecules nearly the plasmonic NPs or those situated in the “hot-spot”

regions experiences a drastic modification of the free-space properties and changes in the excitation and thereby emission rates [40]. Thus SPR is an essential condition for effective enhancement processes.

According to the classical electromagnetic theory, local field enhancement factors for the spheroid with lightning rod factor L_{LR} are given as [41]:

$$\eta_x(\omega) = \frac{\varepsilon_m L_{LR}}{\varepsilon_{Au} - \varepsilon_m + L_{LR}\left(\varepsilon_m + i\,\frac{4\pi^2 V}{\lambda^3}\,(\varepsilon_m - \varepsilon_{Au})\right)} \qquad (8)$$

$$\eta_{y,z}(\omega) = \frac{\varepsilon_m \frac{2L_{LR}}{L_{LR} - 1}}{\varepsilon_{Au} - \varepsilon_m + \frac{2L_{LR}}{L_{LR} - 1}\left(\varepsilon_m + i\,\frac{4\pi^2 V}{\lambda^3}\,(\varepsilon_m - \varepsilon_{Au})\right)} \qquad (9)$$

where η_x, $\eta_{z,y}$ are the enhancement factors for the electric field vectors directed along the axis of revolution of ellipsoid (x) and perpendicular to this axis, respectively. For a depolarized nano-sphere, $L_{LR} = 3$ and $|\eta(\omega)| = 3\varepsilon_m/(\varepsilon_{Au}+\varepsilon_m)$ where directionally averaged intensity enhancement factor $|\eta(\omega)|^2 = |\eta_x(\omega)|^2 + |\eta_y(\omega)|^2 + |\eta_z(\omega)|^2$. The field enhancement factor, η can defined as the ratio of the amplified local field and the incident field, $|\eta(\omega)| = |E_{loc}|/|E_i|$ [20]. Thus, the electric field around the metal is increased. The effect of this additional excitation field, $E_x = (E_{loc} - E_i)$, is shown in Fig. 7. The localized SPR is dependent on the morphology of the NPs, and so does the magnitude of the local field. The magnitude of the longitudinal SPR is typically much larger than the transverse counterpart. Consequently large local field potency can be generated by increasing the aspect ratio of ellipsoidal metal nanoparticles [41]. Another possible factor responsible for photoluminescence enhancement is coupling of the Eu^{3+} $^5D_0 \rightarrow {}^7F_2$ transition dipoles with resonant plasmon modes in the Au NPs [12].

Table 2 also compares the relative intensity of the green, orange and red emission peaks of each of the nanocomposites. The maximum luminescence enhancement has been found to occur at Au concentration 0.03 wt %. Thus, although the local field enhancement phenomenon can clarify the enhanced red emission of Eu^{3+} ions but it cannot explain the drastic reduction of the emission band of Eu^{3+}. The local field persistently grows with Au^0 concentration until it saturates a very high concentration [20]. The damping of intensity (quenching) of the red fluorescence peak (Fig. 6 curve d and Table 2) at higher Au concentration (0.3 wt %) is due to energy transfer from excited state Eu^{3+} ions to Au^0 NPs ($Eu^{3+} \rightarrow Au^0$) and plasmon re-absorption as a consequence of increased quantity of Au NPs aggregates and overlap of the broad and intense SPR band of Au (SPR = 679 nm) with red emission peak of Eu^{3+} [18,19].

Generally, the integrated intensity ratio between the ED and MD transitions can also be used to measure of the local symmetry. The higher is its value; more would be the distortion from the inversion symmetry [1,3,22,34]. For all the samples, the emission spectra are dominated by the hyper sensitive electric dipole transition $^5D_0 \rightarrow {}^7F_2$ (red emission) over the others. In the present case the electromagnetic interaction due to surface plasmons excitation in the gold particles contributes to the intensity changes and affects ED to MD transition ratios. A convenient way to monitor the changes in crystal field around the RE ions is by the determination of variation of asymmetry ratio (AR) with the particle concentration, where AR is defined as the integrated emission intensity ratio between the $^5D_0 \rightarrow {}^7F_2$ (electric dipole transition) and, $^5D_0 \rightarrow {}^7F_1$ (magnetic dipole transition) [10,18]:

$$AR = \int I\,(^5D_0 \rightarrow {}^7F_2)\, d\gamma \,/\, \int I\,(^5D_0 \rightarrow {}^7F_1)\, d\gamma \qquad (10)$$

The variation in the AR value (Table 2) manifests two effects with nanoparticle concentration — the modifications of the crystal field and the local refractive index around Eu^{3+}

ions. From Table 2 it can also be observed that, the value of AR is more than unity for all the three samples suggesting that the Eu^{3+} ions occupy the acentric crystalline sites. The AR value first increases and then decreases. Interactions among the closely separated Au^0 NPs exhibiting coupled SPR with increase in Au concentration are expected to cause distortion of the crystal field [10,18]. However, the decrease in the asymmetric ratio could be seen as an indication that the crystals are more orderly oriented rather than the randomly oriented. Thus local site symmetry is perturbed by random distribution of Au NPs resulting in well resolved stark splitting of the emission bands due to crystal field effect.

3.9 Advantages of this single-step methodology

Although this versatile single-step approach rules out very accurate control of nanoparticles' sizes and inter-particle distance however it has several attention-grabbing features; (1) A disadvantage of ion-exchange technique is that the RE^{3+} ions diffuse to the solution and are lost from the glass. On the contrary, this methodology does not encounter any such loss; (2) The formation of noble metal NPs is restricted only to about 100 μm thickness from each side of the glass plate where the metal ions can penetrate for conventional ion-exchange technique, but here the yield of Au NPs (number density) is very high since it involves in-situ chemical reduction process. Consequently dramatic enhancements of fluorescence of Eu^{3+} (RE) ions are obtained; (3) the methodology being simple, it is scalable up to reasonably a large quantities of materials and bulk glasses embedded with Au NPs (a new generation usable nanomaterials) can be obtained. Here is there is also no possibility of sample damage due to exposure to high intensity radiation; (4) Another disadvantage involving the conventional nucleation and nanoparticle growth processes allow plasmon tuning only after prolonged heat treatment at considerably high

temperatures which hinders fabrication of metal-doped low softening glasses. This problem can be overcome here, i.e. low softening antimony oxide glasses containing metal NPs has been synthesized; (5) the size and relative separation of the Au NPs can be partially restricted by controlling the $HAuCl_4$ concentration of the batch; (6) such stable luminescent dichroic nanocomposites are promising as polarizers, high quality display devices (LCDs) and solar cell application particularly due to the dichroic behavior as well as intense deep-red fluorescence having a narrow FWHM (7.5 nm); (7) all the NCs have brilliant dichroic color and can also be used for decorative purposes; (8) other interesting optical applications may be due to dichroic behavior and enhanced non-linearities caused by elliptical NPs with intensified local electric fields around them.

4. Conclusions

The work demonstrated here exploits the plasmonic enhancement effect in a new dichroic antimony based glass K_2O-B_2O_3-Sb_2O_3 (KBS) nanocomposites co-embedding europium (Eu^{3+}) ions and gold (Au^0) nanoparticles synthesized by a versatile, single-step melt-quench technique involving selective thermochemical reduction without using any external reducing agent. The UV-visible absorption spectra show pronounced surface plasmon resonance (SPR) band characteristic of nano sized Au^0 in addition to the distinctive absorption peaks of Eu^{3+} ion. All the nanocomposites exhibit dichroic behavior due to elliptical shape of Au^0 nanoparticles having aspect ratio about 1.2. The presence of plasmonic metallic surfaces or nanoparticles in the vicinity of the RE ions dramatically alters the luminescence emission and absorption properties of the RE ions. Under excitation at 393 nm and in presence of Au^0 concentration of 0.03 wt %, the $^5D_0 \rightarrow {}^7F_2$ electric dipole transition undergoes distinct stark splitting (617 and 640 nm deep-

red emission) and a remarkable enhancement of about 8 folds. The enhancement effect has been interpreted due to local field enhancement (LEF) induced by Au^0 SPR. Besides, the ratio of the red $^5D_0 \rightarrow {}^7F_2$ electric dipole to orange $^5D_0 \rightarrow {}^7F_1$ magnetic dipole transition has been found to be very high (11.4) which suggests the potential of Eu^{3+}:Au doped in KBS antimony glass as a potential red laser source. We believe that this would bring new outlook in the area of metal-RE-glass hybrid nanocomposites.

Acknowledgements

TS expresses sincere gratitude to the financial support of the Council of Scientific and Industrial Research (CSIR), New Delhi in the form of NET-SRF under sanction number 31/015(0060)/2007-EMR-1. The authors gratefully thank Director of this institute for his kind permission to publish this paper. The technical supports provided by the infrastructural facility of this institute and Unit of Nano Sc & Tech (TEM), IACS, Kolkata are also thankfully acknowledged.

References

[1] K. Pátek, Glass Lasers, Butterworth, London, (1970).

[2] B.S. Richards, Luminescent layers for enhanced silicon solar cell performance: Down-conversion, Sol. Energy Mater. Sol. Cells 90 (2006) 1189–1207.

[3] A. Kumar, D. K. Rai, S. B. Rai, Optical studies of Eu^{3+} ions doped in tellurite glass, Spectrochim. Acta A 58 (2002) 2115-2125

[4] P. N. Prasad, Nanophotonics, Wiley, New Jersey, (2004), pp. 129-151.

[5] M. Eichelbaum, K. Rademann, Plasmonic enhancement or energy transfer? On the luminescence of gold-, silver-, and lanthanide-doped silicate glasses and its potential for light-emitting devices, Adv. Funct. Mater. 19 (2009) 1–8.

[6] S. M. Lee, K. C. Choi, Enhanced emission from $BaMgAl_{10}O_{17}:Eu^{2+}$ by localized surface plasmon resonance of silver particles, Opt. Exp. 18 (2010) 12144-12152.

[7] M. Mattarelli, M. Montagna, K. Vishnubhatla, A. Chiasera, M. Ferrari, G. C. Righini, Mechanisms of Ag to Er energy transfer in silicate glasses: A photoluminescence study, Phys. Rev. B 75 (2007)125102.

[8] J. Z. Zhang, Optical properties and spectroscopy of nanomaterials, World Scientific Publishing Co. Pte. Ltd., Singapore, (2009).

[9] O. L. Malta, P. A. Santa-Cruz, G. F. De Sá, F. Auzel, Fluorescence enhancement induced by the presence of small silver particles in Eu^{3+} doped materials, J. Lumin. 33 (1985) 261-272.

[10] T. Hayakawa, S. T. Selvan, M. Nogami, Remarkable influence of silver islands on the enhancement of fluorescence from Eu^{3+} ion-doped silica gels, J. Phys. Chem. B 103 (1999) 7064-7067.

[11] C. Strohhöfer, A. Polman, Silver as a sensitizer for erbium, Appl. Phys. Lett. 81 (2002) 1414 (3 pp).

[12] Z. Pan, A. Ueda, R. Aga Jr., A. Burger, R. Mu, S.H. Morgan, Spectroscopic studies of Er^{3+} doped Ge-Ga-S glass containing silver nanoparticles, J. Non-Cryst. Solids 356 (2010) 1097-1101.

[13] M. Fukushima, N. Managaki, M. Fujii, H. Yanagi, S. Hayashi, Enhancement of 1.54-μm emission from Er-doped sol-gel SiO_2 films by Au-nanoparticles doping, J. Appl. Phys. 98 (2005) 24316 (4 pp.).

[14] L. R. P. Kassab, D. S. da Silva, R. de Almeida, C. B. de Araújo, Photoluminescence enhancement by gold nanoparticles in Eu^{3+} doped GeO_2–Bi_2O_3 glasses, Appl. Phys. Lett. 94 (2009) 101912.

[15] R. de Almeida, D. M. da Silva, L. R.P. Kassab, and C. B. de Araújo, Eu^{3+} luminescence in tellurite glasses with gold nanostructures, Optics Commun. 281 (2008) 108–112

[16] G. E. Malashkevich, A. V. Semchenko, A. A. Sukhodola, A. P. Stupak, A. V. Sukhodolov, B. V. Plyushch, V. V. Sidskiĭ, G. A. Denisenko, Influence of silver on the Sm^{3+} luminescence in "aerosil" silica glasses, Phys. Solid State 50 (2008) 1464–1472.

[17] F. Gonella and P. Mazzoldi, Metal nanocluster composite glasses, In: Handbook of Nanostructured Materials and Nanotechnology, H. S. Nalwa (editor), Academic Press, San Diego, Vol 4, 2000, pp. 81-158.

[18] H. Nabika, S. Deki, Enhancing and quenching functions of silver nanoparticles on the luminescent properties of europium complex in the solution phase, J. Phys. Chem. B 107 (2003) 9161-9164.

[19] Y. Wang, J. Zhou, T. Wang, Enhanced luminescence from europium complex owing to surface plasmon resonance of silver nanoparticles, Mater. Lett. 62 (2008) 1937–1940.

[20] F. Le, D. W. Brandl, Y. A. Urzhumov, H. Wang, J. Kundu, N. J. Halas, J. Aizpurua, P. Nordlander, Metallic nanoparticle arrays: A common substrate for both surface-enhanced raman scattering and surface-enhanced infrared absorption, ACS Nano 2 (2008) 707-718.

[21] T. Som, B. Karmakar, Structure and properties of low-phonon antimony glasses and nano glass-ceramics in K_2O-B_2O_3-Sb_2O_3 system, J. Non-Cryst. Solids 356 (2010) 987–999.

[22] T. Som, B. Karmakar, Optical properties of Eu^{3+}-doped antimony-oxide-based low phonon disordered matrices, J. Phys.: Condens. Mat. 22 (2010) 035603 (11 pp.).

[23] CRC Handbook of Chemistry and Physics, D. R. Lide, CRC press, Boca Raton, 75th edn, 1975, pp. 8-21-34.

[24] B. D. Cullity, Elements of X-ray diffraction, Addison-Wesley Publishing Co. California, 1978, p. 102.

[25] W. T. Carnall, P. R. Fields, K. Rajnak, Electronic energy levels in the trivalent lanthanide aquo ions. IV. Eu^{3+}, J. Chem. Phys. 49 (1968) 4450-4455.

[26] K. L. Kelly, E. Coronado, L. L. Zhao, and G. C. Schatz, The optical properties of metal nanoparticles: The influence of size, shape, and dielectric environment, J. Phys. Chem. B 107 (2003) 668-677.

[27] W. A. Weyl, Colored Glasses, Society of Glass Technology, Sheffield, 1999, pp. 366-400.

[28] M. Kaempfe, T. Rainer, K. -J. Berg, G. Seifert, H. Graener, Ultrashort laser pulse induced deformation of silver nanoparticles in glass, Appl. Phys. Lett. 74 (1999) 1200-1202.

[29] H. G. Silva-Pereyra, J. Arenas-Alatorre, L. Rodriguez-Fernández, A. Crespo-Sosa, J. C. Cheang-Wong, J. A. Reyes-Esqueda, Alicia Oliver, High stability of the crystalline configuration of Au nanoparticles embedded in silica under ion and electron irradiation, J. Nanopart. Res. 12 (2010) 1787-1795.

[30] E. H. Land, Light polarizer and process of manufacture, US Patent 2,319,816 (1943).

[31] H. Hofmeister, W. –G. Drost, and A. Berger, Oriented prolate silver particles in glass-characteristics of novel dichroic polarizers, Nanostruct. Mater. 12 (1999) 207-210.

[32] J. Pérez-Juste, I. Pastoriza-Santos, L. M. Liz-Marzán, and P. Mulvaney, Gold nanorods: Synthesis, characterization and applications, Coord. Chem. Rev. 249 (2005) 1870–1901.

[33] K. –S. Lee, M. A. El-Sayed, Gold and silver nanoparticles in sensing and imaging: sensitivity of plasmon response to size, shape, and metal composition, J. Phys. Chem. B 110 (2006) 19220-19225.

[34] D. Zhao, X. Qiao, X. Fan, and M. Wang, Local vibration around rare earth ions in SiO_2–PbF_2 glass and glass ceramics using Eu^{3+} probe, Physica B 395 (2007) 10–15.

[35] M. Langlet, C .Coutier, W. Meffre, M. Audier, J. Fick, R. Rimet, B. Jacquier, Microstructural and spectroscopic study of sol-gel derived Nd-doped silica glasses, J. Lumin. 96 (2002) 295-309.

[36] J. Shin, K. Jang, K. –S. Lim, I. –B. Sohn, Y. –C. Noh, and J. Lee, Formation and control of Au and Ag nanoparticles inside borate glasses using femtosecond laser and heat treatment, Appl. Phys. A 93 (2008) 923–927.

[37] J. P. Wilcoxon, J. E. Martin, F. Parasapour, B. Wiedenman, D. F. Kelly, Photoluminescence from nanosize gold clusters, J. Chem. Phys. 108 (1998) 9137-9143.

[38] J. A. Jiménez, S. Lysenko, H. Liu, Photoluminescence via plasmon resonance energy transfer in silver nanocomposite glasses, J. Appl. Phys. 104 (2008) 054313.

[39] D. Manikandan, S. Mohan, K. G. M. Nair, Absorption and luminescence of silver nanocomposite soda-lime glass formed by Ag^{+}–Na^{+} ion-exchange, Mater. Res. Bull. 38 (2003) 1545-1550.

[40] M. Wu, J. R. Lakowicz, C. D. Geddes, Enhanced lanthanide luminescence using silver nanostructures: Opportunities for a new class of probes with exceptional spectral characteristics, J. Fluores. 15 (2005) 53-59.

[41] O. P. Varnavski, T. Goodson, M. B. Mohamed, M. A. El-Sayed, Femtosecond excitation dynamics in gold nanospheres and nanorods, Phys. Rev. B 72 (2005) 235405.

Table 1
Composition and some physical properties of the nanocomposites

Glass/ composite no.	Composition[a] (wt %)		Density, ρ ($g.cm^{-3}$)	Transmitted color	Reflected color	SPR band, λ_{max} (± 0.1, nm)	Particle diameter (D) calculated from Eq. 1 (±1, nm)
	Eu_2O_3	Au					
E	0.3	-	4.569	yellow	-	-	-
EG1	0.3	0.003	4.571	green	brown	609	10
EG2	0.3	0.03	4.578	bluish-green	brown	624	17
EG3	0.3	0.3	4.595	blue	brown	679	26
G	-	0.3	4.587	blue	brown	681	-

[a] Base glass composition (mol %) 15 K_2O-15B_2O_3-70Sb_2O_3. All concentrations of Eu_2O_3 and Au are in excess.

Table 2
Some calculated properties and variation of relative intensity of upconversion fluorescence bands with Au concentration in the nanocomposites

Topic	Corresponding values				
Glass/composite number	E	EG1	EG2	EG3	G
Fluorescence (λ_{ex} = 393 nm)					
ratio of I($^5D_0 \rightarrow {}^7F_1$) at different concentration, ± 0.02	1	1.6	1.7	1.4	-
ratio of I($^5D_0 \rightarrow {}^7F_2$) at different concentration, ± 0.02	1	4.1	8.2	3.0	-
ratio of I($^5D_0 \rightarrow {}^7F_1$) : I($^5D_0 \rightarrow {}^7F_2$) at different concentration, ± 0.02	1:2.2	1:5.2	1:11.4	1:4.8	-
Asymmetry Ratio (AR)	2.2	5.2	11.4	4.8	

Figure Captions

Fig. 1. (Color online) Dichroic behavior of Eu^{3+}:Au glass nanocomposite EG3: (a) blue in transmitted light and (b) brown in reflected light (for composition see Table 1).

Fig. 2. XRD patterns of nanocomposites (a) E, (b) EG1, (a) EG3 and (d) EG4 (for composition see Table 1).

Fig. 3. (a) TEM image of the nanocomposite EG1 showing elliptical Au NPs having an aspect ratio of about 1.2 and (b) SAED of Au nanoparticle (for composition see Table 1).

Fig. 4. UV-Vis-NIR absorption spectra of (a) E, (b) EG1, (c) EG2 and (d) EG3 in the range of 380-1100 nm showing the various transitions of Eu^{3+} arising from the ground state (inset shows the magnification of curve (a)) and the SPR positions of nano Au (for composition see Table1), (thickness: 2 mm).

Fig. 5. Excitation spectrum of (a) E and (b) EG2 with emission at λ_{em} = 617 nm, (cps is cycles per second) (for composition see Table 1).

Fig. 6. Fluorescence spectra of (a) E, (b) EG1, (c) EG2 and (d) EG3, under excitation wavelength at λ_{ex} = 393 nm (for composition see Table 1 and amplification ratio Table 2). The bases of the emission curves b, c and d have been uplifted for clear visibility.

Fig. 7. (Color online) Partial energy level diagram of Eu^{3+} ion in $15K_2O$-$15B_2O_3$-$70Sb_2O_3$ (mol %) glass showing ground state absorption (GSA) and local field enhancement (LFE, E_x) by surface plasmon resonance of Au^0 nanoparticles (R and NR represent the radiative and non-radiative transitions respectively).

Fig. 8. Plot of integrated intensity as a function of concentration of Au (wt%) for MD $^5D_0 \rightarrow {}^7F_1$ orange and ED $^5D_0 \rightarrow {}^7F_2$ red emission bands. Maximum amplification of the orange and red emissions are found to be about 1.7 and 8.2 folds respectively for nanocomposite EG2 (for compositions see Table 1 and amplification ratio Table 2). The lines are drawn to guide the eye.

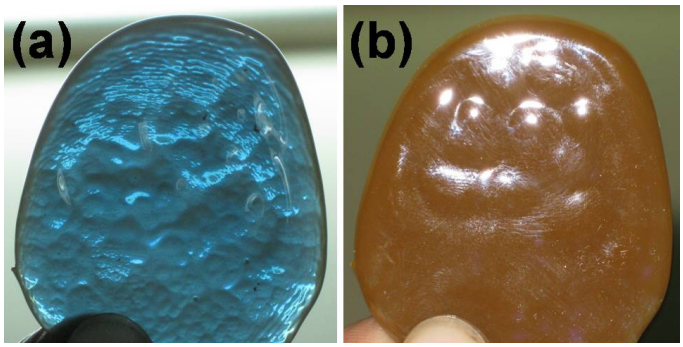
(a)
(b)

Fig. 1.

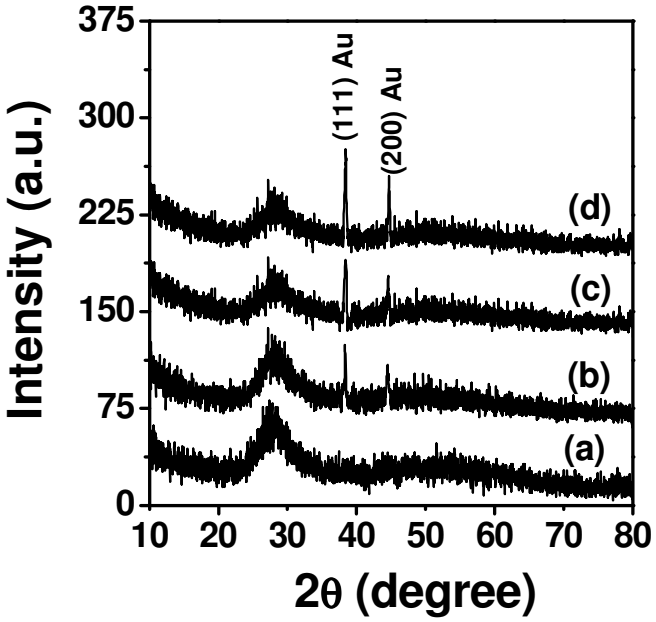
Intensity (a.u.)
375
300
225
150
75
0
(111) Au
(200) Au
(d)
(c)
(b)
(a)
10
20
30
40
50
60
70
80
2θ (degree)

Fig. 2.

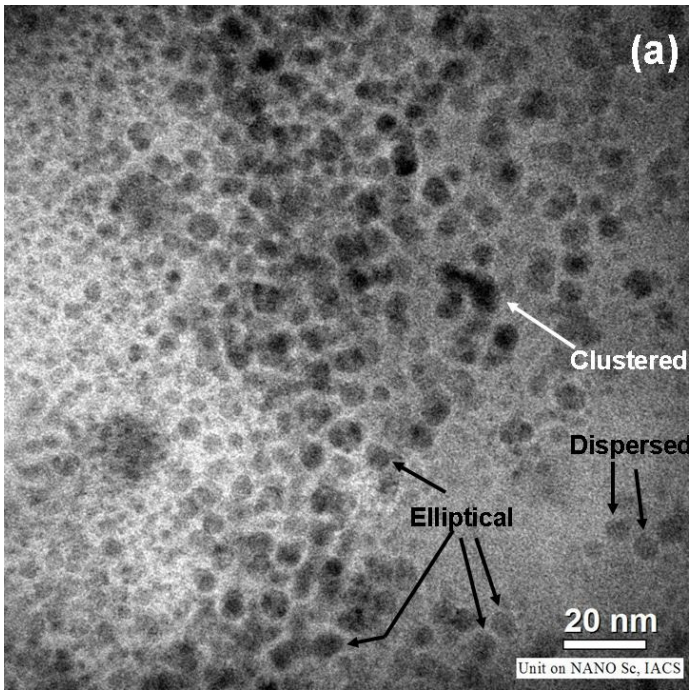
(a)
Clustered
Dispersed
Elliptical
20 nm
Unit on NANO Sc, IACS

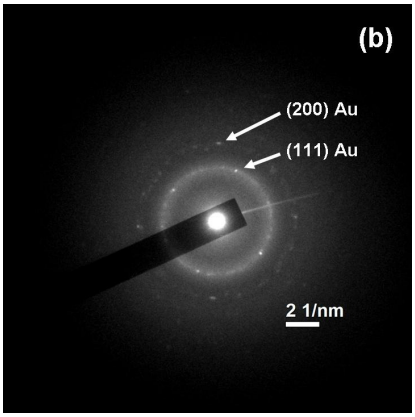
(b)
(200) Au
(111) Au
2 1/nm

Fig. 3 (a) and (b).

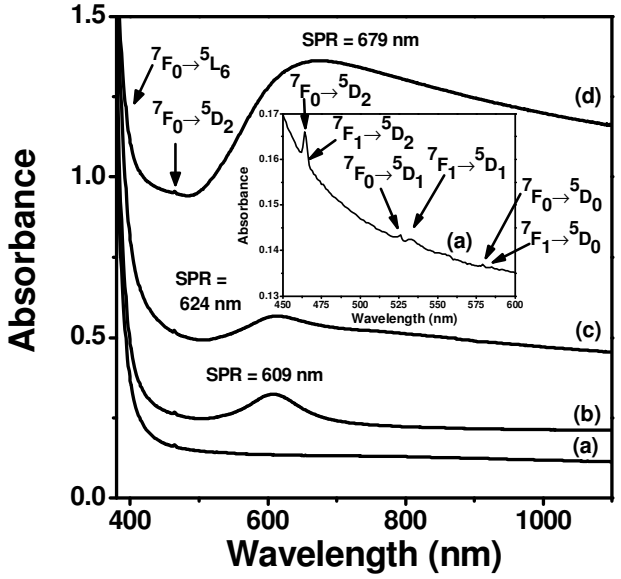
Absorbance
Wavelength (nm)
SPR = 679 nm
SPR = 624 nm
SPR = 609 nm
$^7F_0 \rightarrow {}^5L_6$
$^7F_0 \rightarrow {}^5D_2$
$^7F_1 \rightarrow {}^5D_2$
$^7F_0 \rightarrow {}^5D_1$
$^7F_1 \rightarrow {}^5D_1$
$^7F_0 \rightarrow {}^5D_0$
$^7F_1 \rightarrow {}^5D_0$
(a)
(b)
(c)
(d)

Fig. 4.

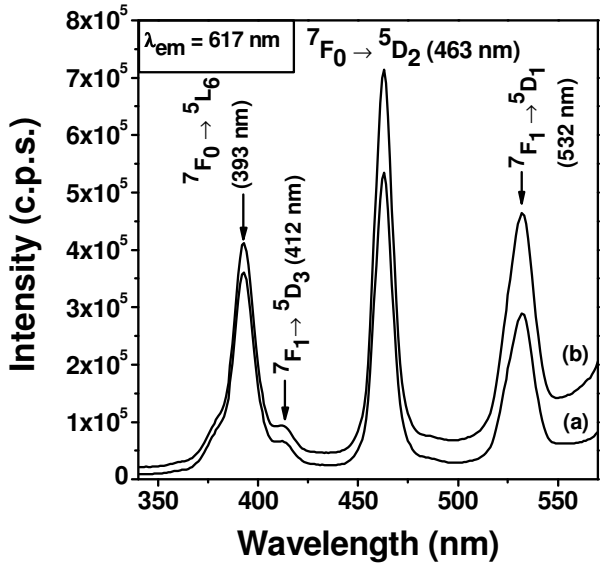
Intensity (c.p.s.)
Wavelength (nm)
λ_{em} = 617 nm
$^7F_0 \rightarrow {}^5D_2$ (463 nm)
$^7F_0 \rightarrow {}^5L_6$ (393 nm)
$^7F_1 \rightarrow {}^5D_3$ (412 nm)
$^7F_1 \rightarrow {}^5D_1$ (532 nm)
(a)
(b)

Fig. 5.

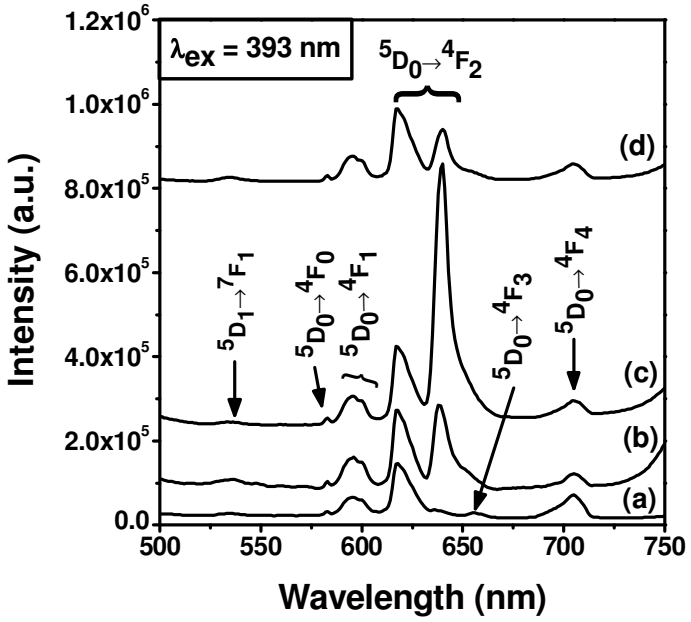
λex = 393 nm
5D0→4F2
(d)
(c)
(b)
(a)
5D1→7F1
5D0→4F0
5D0→4F1
5D0→4F3
5D0→4F4
Intensity (a.u.)
Wavelength (nm)
1.2x10^6
1.0x10^6
8.0x10^5
6.0x10^5
4.0x10^5
2.0x10^5
0.0
500
550
600
650
700
750

Fig. 6.

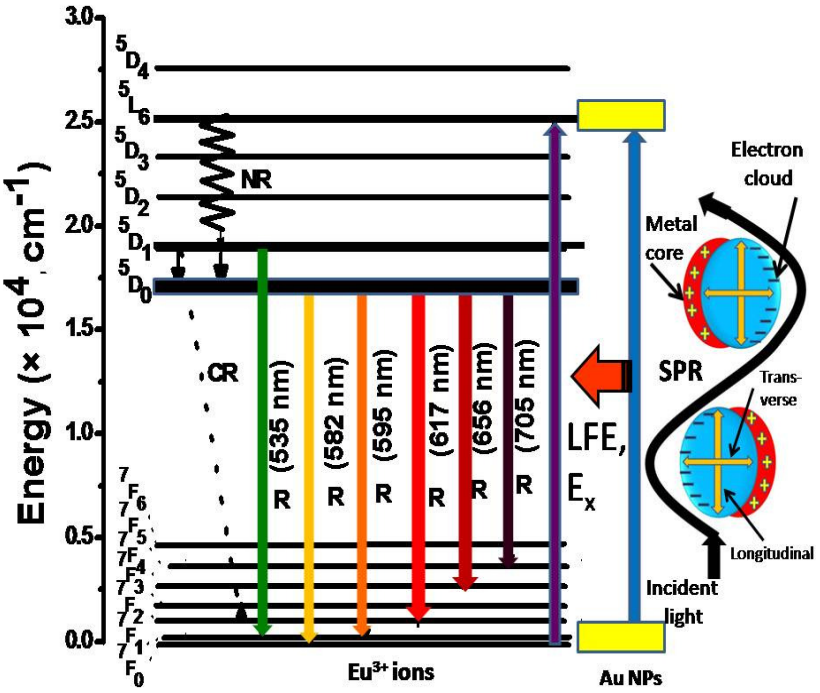
Energy (× 10^4 cm^-1)
3.0
2.5
2.0
1.5
1.0
0.5
0.0
5D4
5L6
5D3
5D2
5D1
5D0
NR
CR
(535 nm)
(582 nm)
(595 nm)
(617 nm)
(656 nm)
(705 nm)
R
LFE,
Ex
7F6
7F5
7F4
7F3
7F2
7F1
7F0
Eu3+ ions
Au NPs
Electron cloud
Metal core
SPR
Trans-verse
Longitudinal
Incident light

Fig. 7.

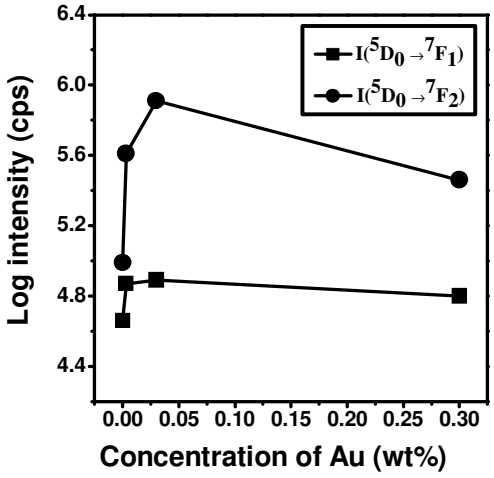
Log intensity (cps)
6.4
6.0
5.6
5.2
4.8
4.4
0.00
0.05
0.10
0.15
0.20
0.25
0.30
Concentration of Au (wt%)
I(5D0 → 7F1)
I(5D0 → 7F2)

Fig. 8.